International Journal of Solids and Structures 49 (2012) 1947–1960

Contents lists available at SciVerse ScienceDirect

International Journal of Solids and Structures

journal homepage: www.elsevier.com/locate/ijsolstr

Effect of spherical micro-voids in shape memory alloys subjected to uniaxial loading

J.S. Olsen, Z.L. Zhang *

Department of Structural Engineering, Norwegian University of Science and Technology (NTNU), N-7491 Trondheim, Norway

ARTICLE INFO

Article history:
Received 21 November 2011
Received in revised form 4 February 2012
Available online 16 April 2012

Keywords:
Shape memory alloys
Superelastic–plastic
Micro-voids
Constitutive model

ABSTRACT

In this study the effect of micro-voids on the superelastic–plastic behavior of shape memory alloys is investigated. A new constitutive model for porous shape memory alloys, based on the Gurson–Tvergaard–Needleman formulation, is proposed. The model is able to reproduce both forward and reverse stress induced phase transformation, as well as plastic deformation. In addition, the model accounts for the presence of micro-voids and void-growth through a void volume fraction. A one dimensional implementation has been conducted, and results from the new constitutive model is compared with finite element unit-cell analyses. The model does well in reproducing results from unit-cells with void volume fractions $f_0 < 0.05$. However, some discrepancy is found for void volume fractions $f_0 \geqslant 0.05$ that can be attributed to the highly inhomogeneous stress field in the unit-cells which the new model does not account for. The main results show that even for relatively small micro-voids the stress at which transformation and plastic yielding is initiated is lowered. Also, the presence of micro-voids leads to a narrowing of the stress–strain hysteresis which affects the amount of energy dissipated during a superelastic cycle.

1. Introduction

In recent years, there have been an increased focus on failure of shape memory alloys. The main efforts have been invested in understanding the fatigue behavior (McKelvey and Ritchie, 2001; Robertson et al., 2007; Robertson and Ritchie, 2007; Gollerthan et al., 2008), but there have also been conducted studies devoted to understand what fracture mechanisms are dominating for shape memory alloys (see e.g. Gall et al., 2001; Chen et al., 2005). The results found in the literature do not provide distinct conclusions, but rather show that fracture of shape memory alloys is governed by several mechanisms.

Microstructural aspects have been shown to significantly affect the fracture behavior of single crystalline NiTi. In a study Gall et al. (2001) found that governing fracture mechanisms ranged from almost pure cleavage to a combination of cleavage and void-growth, depending on the grain-orientation and presence and size of second-phase precipitates. In the same study, fracture of polycrystalline NiTi was investigated and it was concluded that one of the main fracture mechanisms for the investigated material is ductile rupture through void-growth and coalescence. Other authors have also shown results which indicate that ductile fracture mechanisms are present during the fracture process of shape memory alloys (Vaidyanathan et al., 2000; Wang et al., 2009). It is well established that the nucleation, growth and coalescence of micro-voids play a crucial role in ductile rupture (Rice and Tracey, 1969; Gurson, 1977; Koplik and Needleman, 1988; Zhang et al., 2000).

The effect of pores on shape memory alloy behavior has been investigated by various authors (Qidwai et al., 2001; Entchev and Lagoudas, 2002, 2004; Nemat-Nasser et al., 2005; Panico and Brinson, 2008). Qidwai et al. (2001) compared three-dimensional unit-cell finite element analyses with results from an averaging micromechanics method based on the Mori–Tanaka method; Entchev and Lagoudas (2002) developed a constitutive model accounting for the effect of pores on superelastic shape memory alloy, which has been extended to account for transformation induced plasticity by Lagoudas and Entchev (2004) and Entchev and Lagoudas (2004). The latter works are also based on an averaging technique where it is assumed that the material consists of pores, which are considered to be inhomogeneities with zero stiffness, and a dense matrix with superelastic–plastic properties; Panico and Brinson (2008) simulated the effect of pores on the shape memory alloy behavior by introducing a random distribution of elements with zero stiffness in a representative volume.

The common denominator for all of the works conducted on porous shape memory alloys is that they consider materials with large porosity (10–60%). To the author's knowledge no studies have been conducted on the superelastic–plastic shape memory alloys with void volume fractions that is less than 10%. The existence of micro-voids might influence the fracture behavior of shape memory alloys, as a first step we aim to investigate what effect the

* Corresponding author.
E-mail address: Zhiliang.Zhang@ntnu.no (Z.L. Zhang).

0020-7683/$ - see front matter © 2012 Elsevier Ltd. All rights reserved.
http://dx.doi.org/10.1016/j.ijsolstr.2012.03.041

micro-voids can have on the behavior of shape memory alloys prior to fracture.

In this work, a new superelastic–plastic constitutive model based on the Gurson–Tvergaard–Needleman model is proposed for shape memory alloys containing micro-voids. The model is able to reproduce the stress–strain hysteresis, the stress drop due to the presence of micro-voids and the void-growth in the material. The model is implemented in Matlab for a one dimensional stress state using a forward Euler integration scheme. Results from the new model are compared with results from finite element unit cell analyses conducted with the commercial finite element software Abaqus. The effect of micro-voids on the superelastic–plastic behavior of shape memory alloys is investigated.

In the following, a thorough description of the constitutive model will be given in Section 2. Section 3 outlines the finite element procedures and set up for the unit cell analyses, and shows the material parameter fitting between the new constitutive model and the finite element analyses. Results and discussion are presented in Section 4 before conclusions are given in Section 5.

2. Constitutive model accounting for effect of micro-voids in shape memory alloys

Deformation of superelastic shape memory alloys leads to a stress induced phase transformation from austenite to martensite. Generally, up to 24 martensite variants may form in a shape memory alloy (Otsuka and Ren, 2005). However, when the material is deformed in the austenite phase, only one variant, which is oriented energetically most favorable relative to the direction of the stress, will form (Brinson, 1993). It is therefore convenient to simplify the problem to account for only one martensite variant. This simplification is similar to the approaches found in several other superelastic constitutive models, see e.g. (Brinson, 1993; Auricchio and Taylor, 1997). Represented through their volume fractions, the austenite and martensite phase, denoted ξ_a and ξ_m respectively, have to satisfy the following conditions

$$\xi_a + \xi_m = 1, \tag{1}$$

and

$$d\xi_a + d\xi_m = 0, \tag{2}$$

Eq. (1) allows the austenite volume fraction to be expressed through the martensite volume fraction as

$$\xi_a = 1 - \xi_m. \tag{3}$$

In the following, ξ is used without subscript and denotes the martensite volume fraction.

As martensite transformation in shape memory alloys is considered a thermoelastic process (Funakubo, 1987), the mechanical behavior is influenced by both temperature and stress. In this work we consider the transformation as an isothermal process, i.e. the temperature is constant and only the mechanical contribution is considered. This allows us to construct a constitutive relation on the form

$$d\boldsymbol{\sigma} = \mathbb{C} : d\boldsymbol{\varepsilon}^{el}. \tag{4}$$

where $d\boldsymbol{\sigma}$ is the incremental 2nd-order stress tensor, $\mathbb{C}$ is the 4th-order isotropic elasticity tensor and $d\boldsymbol{\varepsilon}^{el}$ is the incremental 2nd-order elastic strain tensor. Considering the superelastic–plastic deformation to be a three stage deformation, the total strain increment, $d\boldsymbol{\varepsilon}$, can be expressed through an additive decomposition on the form

$$d\boldsymbol{\varepsilon} = d\boldsymbol{\varepsilon}^{el} + d\boldsymbol{\varepsilon}^{tr} + d\boldsymbol{\varepsilon}^{pl}, \tag{5}$$

with $d\boldsymbol{\varepsilon}^{tr}$ and $d\boldsymbol{\varepsilon}^{pl}$ as the incremental 2nd-order transformation and plastic strain tensors, respectively. Usually the yield stress needed to initiate plastic deformation through dislocation movement is higher than the critical stress to initiate martensite transformation (Yan et al., 2003). It is therefore convenient to treat the two cases separately. Accordingly, the stress increment can be written for $\xi < 1$ and $\xi = 1$, respectively:

$$d\boldsymbol{\sigma} = \mathbb{C} : (d\boldsymbol{\varepsilon} - d\boldsymbol{\varepsilon}^{tr}), \quad \xi < 1 \tag{6}$$

$$d\boldsymbol{\sigma} = \mathbb{C} : (d\boldsymbol{\varepsilon} - d\boldsymbol{\varepsilon}^{pl}), \quad \xi = 1. \tag{7}$$

2.1. Martensite transformation

In this work, the goal is to establish a constitutive relation that accounts for the effect of micro-voids during martensite transformation as well as plastic deformation. Simultaneously the model should inhibit the ability to reproduce the superelastic hysteresis that separates shape memory alloys from conventional materials. In order to accomplish this, a transformation potential similar to the Gurson–Tvergaard–Needleman potential (Gurson, 1977; Tvergaard, 1981; Tvergaard and Needleman, 1984) has been adopted. For forward transformation (i.e. transformation from austenite to martensite) we have a potential on the form

$$\Phi^{for}(\boldsymbol{\sigma}, f, \xi) = \frac{q^2}{\sigma_f^{for\,2}} + 2k_1 f \cosh\left(\frac{3k_2 p}{2\sigma_f^{for}}\right) - \left(1 + (k_1 f)^2\right) = 0, \tag{8}$$

where $q(\boldsymbol{\sigma}) = \sqrt{\frac{3}{2}\mathbf{S} : \mathbf{S}}$ and $p(\boldsymbol{\sigma}) = \frac{1}{3}\mathrm{tr}(\boldsymbol{\sigma})$ are the equivalent Von Mises stress and hydrostatic stress, respectively. $\mathbf{S}$ is the deviatoric stress tensor and $\sigma_f^{for} = \sigma_f^{for}(\xi)$ is the transformation flow stress for forward transformation. k_1 and k_2 are constants introduced to the original Gurson model by Tvergaard (1981) and Tvergaard and Needleman (1984) to better describe the stress carrying capacity during void-growth and coalescence. The void volume fraction, f, and ξ are chosen as internal variables. Similarly a potential, $\Phi^{rev}(\boldsymbol{\sigma}, f, \xi)$, can be written for reverse transformation (i.e. transformation from martensite to austenite due to unloading) by substituting σ_f^{for} with $\sigma_f^{rev} = \sigma_f^{rev}(\xi)$ which is the transformation flow stress for reverse transformation.

It is assumed that the transformation strain increment is proportional to the transformation potential normal, $\partial\Phi/\partial\boldsymbol{\sigma}$, following the notation of Auricchio and Taylor (1997) and Yan et al. (2003), the normality rule gives for forward transformation

$$d\boldsymbol{\varepsilon}^{tr} = \beta^{for} d\xi \frac{\partial \Phi^{for}}{\partial \boldsymbol{\sigma}}, \tag{9}$$

In Eq. (9) β^{for} is a material parameter which is connected to the transformation length, ϵ_L, and the transformation flow stress. This point will be revisited at a later stage. $d\xi$ is the martensite volume fraction increment which needs to be determined. In order to describe the transformation strain for reverse transformation, the potential Φ^{rev} and a material parameter β^{rev} is employed in Eq. (9). Further it has been used that (not separating between forward and reverse transformation)

$$\frac{\partial \Phi}{\partial \boldsymbol{\sigma}} = \frac{\partial \Phi}{\partial q}\frac{\partial q}{\partial \boldsymbol{\sigma}} + \frac{\partial \Phi}{\partial p}\frac{\partial p}{\partial \boldsymbol{\sigma}} = \frac{3\mathbf{S}}{\sigma_f^2} + \frac{k_1 k_2 f}{\sigma_f}\sinh\left(\frac{3k_2 p}{2\sigma_f}\right)\mathbf{I}. \tag{10}$$

It is in this work assumed that the evolution of the void volume fraction during forward transformation is determined by the growth of existing micro-voids (nucleation of new micro-voids is ignored). In this work, phase transformation is phenomenologically treated to behave similar to plastic deformation, which is consistent with the work presented by Lubliner and Auricchio (1996). Following this assumption, and the governing practice regarding void-growth (Gurson, 1977; Zhang et al., 2000), the effect of elastic volumetric strains is considered negligible. Therefore, as long as no

plastic deformation has developed, the change in the void volume fraction is determined by transformation incompressibility:

$$df = (1-f)\mathrm{tr}(d\boldsymbol{\varepsilon}^{tr}) = (1-f)d\varepsilon_V^{tr}. \tag{11}$$

where $d\varepsilon_V^{tr} = d\boldsymbol{\varepsilon}^{tr} : \mathbf{I}$ is the volumetric transformation strain. Using Eq. (9) in Eq. (11) yields for forward transformation

$$df^{for} = (1-f)\beta^{for}\frac{\partial \Phi^{for}}{\partial \boldsymbol{\sigma}} : \mathbf{I}d\xi = \beta^{for}h_f^{for}d\xi. \tag{12}$$

when modeling martensite transformation kinetics, it is common to use an empirically fitted relation to describe the martensite evolution (Tanaka, 1986; Brinson, 1993; Auricchio and Taylor, 1997). In this work, motivated by the approach of Yan et al. (2003), the consistency condition $d\Phi^{for} = d\Phi^{rev} = 0$ is used in order to establish an evolution equation for the martensite volume fraction. Accordingly the change in martensite during forward transformation can be expressed as

$$d\xi = \frac{\frac{\partial \Phi^{for}}{\partial \boldsymbol{\sigma}} : \mathbb{C} : d\boldsymbol{\varepsilon}}{\frac{\partial \Phi^{for}}{\partial \boldsymbol{\sigma}} : \mathbb{C} : \frac{\partial \Phi^{for}}{\partial \boldsymbol{\sigma}}\beta^{for} - \frac{\partial \Phi^{for}}{\partial f}h_f^{for}\beta^{for} - \frac{\partial \Phi^{for}}{\partial \sigma_f^{for}}\frac{\partial \sigma_f^{for}}{\partial \xi}} \tag{13}$$

$$= \mathbf{h}_{\xi}^{for} : d\boldsymbol{\varepsilon}. \tag{14}$$

Only the expressions relating to forward transformation is given for both the change in void volume fraction and the martensite evolution. Similar expressions can easily be established for reverse transformation by substituting the transformation potential, Φ^{for}, the material parameter, β^{for}, and the transformation flow stress, σ_f^{for} so that they are appropriate for reverse transformation. In Eq. (13) it has been used that (not distinguishing forward and reverse transformation)

$$\frac{\partial \Phi}{\partial f} = 2k_1\cosh\left(\frac{3k_2p}{2\sigma_f}\right) - 2k_1^2 f \tag{15}$$

and

$$\frac{\partial \Phi}{\partial \sigma_f} = -\frac{3k_1k_2fp\sigma_f\sinh\left(\frac{3k_2p}{2\sigma_f}\right) + 2q^2}{\sigma_f^3}. \tag{16}$$

$\partial\sigma_f/\partial\xi$ governs the transformation hardening. It is assumed that the Kuhn–Tucker conditions

$$d\xi \geqslant 0, \quad d\Phi^{for} \leqslant 0, \quad d\xi d\Phi^{for} = 0 \tag{17}$$

$$d\xi \leqslant 0, \quad d\Phi^{rev} \geqslant 0, \quad d\xi d\Phi^{rev} = 0 \tag{18}$$

are satisfied for both forward and reverse transformation, respectively.

2.2. Plastic deformation after ended forward transformation

Given that forward transformation has finished ($\xi = 1$), continued loading will lead to an elastic deformation of the martensite phase before plastic deformation by dislocation movement sets in at a given yield stress, σ_y^{pl}. Accounting for micro-voids, the plastic flow potential can be written as (Gurson, 1977; Tvergaard, 1981; Tvergaard and Needleman, 1984)

$$\Phi^{pl}(\boldsymbol{\sigma}, f, \sigma_f^{pl}) = \frac{q^2}{\sigma_f^{pl2}} + 2k_1 f\cosh\left(\frac{3k_2p}{2\sigma_f^{pl}}\right) - \left(1 + (k_1f)^2\right) = 0, \tag{19}$$

Now the void volume fraction, f, and the plastic flow stress, σ_f^{pl}, are chosen as internal variables. Assuming normality, the flow rule gives the incremental second-order plastic strain tensor:

$$d\boldsymbol{\varepsilon}^{pl} = d\lambda\frac{\partial \Phi^{pl}}{\partial \boldsymbol{\sigma}}, \tag{20}$$

where $d\lambda$ is the plastic multiplier, which needs to be determined. As during transformation, void growth is assumed to be determined by growth of existing micro-voids. The change in void volume fraction becomes

$$df = (1-f)\mathrm{tr}(d\boldsymbol{\varepsilon}^{pl}) = (1-f)d\varepsilon_V^{pl}. \tag{21}$$

with $d\varepsilon_V^{pl} = d\boldsymbol{\varepsilon}^{pl} : \mathbf{I}$ as the volumetric plastic strain increment. Inserting Eq. (20) in Eq. (21) yields

$$df = (1-f)d\lambda\frac{\partial \Phi^{pl}}{\partial \boldsymbol{\sigma}} : \mathbf{I} = h_f^{pl}d\lambda. \tag{22}$$

The plastic work rate balance yields

$$\boldsymbol{\sigma} : d\boldsymbol{\varepsilon}^{pl} = (1-f)\sigma_f d\varepsilon_{eq}^{pl} \tag{23}$$

$$\Rightarrow d\varepsilon_{eq}^{pl} = \frac{\boldsymbol{\sigma} : d\boldsymbol{\varepsilon}^{pl}}{(1-f)\sigma_f}. \tag{24}$$

The consistency condition, $d\Phi^{pl} = 0$, yields for the plastic multiplier:

$$d\lambda = \frac{\frac{\partial \Phi^{pl}}{\partial \boldsymbol{\sigma}} : \mathbb{C} : d\boldsymbol{\varepsilon}}{\frac{\partial \Phi^{pl}}{\partial \boldsymbol{\sigma}} : \mathbb{C} : \frac{\partial \Phi^{pl}}{\partial \boldsymbol{\sigma}} - \frac{\partial \Phi^{pl}}{\partial f}h_f^{pl} - \frac{\partial \Phi^{pl}}{\partial \sigma_f^{pl}}h_{\sigma_f^{pl}}} \tag{25}$$

$$= \mathbf{h}_{d\lambda} : d\boldsymbol{\varepsilon}. \tag{26}$$

For a one-dimensional stress state Eq. (25) becomes

$$d\lambda = \frac{\frac{\partial \Phi^{pl}}{\partial \sigma_{11}}Dd\varepsilon_{11}}{\frac{\partial \Phi^{pl}}{\partial \sigma_{11}}D^*\frac{\partial \Phi^{pl}}{\partial \sigma_{11}} - \frac{\partial \Phi^{pl}}{\partial f}h_f^{pl} - \frac{\partial \Phi^{pl}}{\partial \sigma_f^{pl}}h_{\sigma_f^{pl}}} \tag{27}$$

$$= h_{d\lambda}d\varepsilon_{11}. \tag{28}$$

where $h_{\sigma_f^{pl}}$ is the evolution of the plastic flow stress which is determined in Section 2.3. D is the elasticity modulus. It is assumed that the Kuhn–Tucker conditions are satisfied:

$$d\lambda \geqslant 0, \quad d\Phi^{pl} \leqslant 0, \quad d\lambda d\Phi^{pl} = 0. \tag{29}$$

2.3. Hardening rules

In the model suggested in this work, transformation hardening is governed by a relationship between the transformation flow stress and the martensite volume fraction. It is assumed that the hardening mechanisms are the similar for forward and reverse transformation, and for the sake of simplicity the two cases are not separated in the following discussion.

When choosing a hardening rule, several options are available and three approaches are considered herein. As mentioned, $\partial\sigma_f/\partial\xi$ controls the transformation hardening and it has been stated that $\sigma_f = \sigma_f(\xi)$. The simplest option is to assume no hardening, i.e. the transformation flow stress is kept constant throughout the transformation:

$$\sigma_f(\xi) = \sigma_s^{cr} \Rightarrow \frac{\partial \sigma_f}{\partial \xi} = 0. \tag{30}$$

σ_s^{cr} is the critical stress for starting transformation. Generally the critical stresses governing the stress induced martensite transformation are temperature dependent (Brinson, 1993). Since, in this work, the transformation process is considered isothermal, the critical stresses are treated as material constants.

Considering linear hardening, the transformation flow stress can be expressed as

$$\sigma_f(\xi) = \sigma_s^{cr} + \Delta\sigma^{cr}\xi \Rightarrow \frac{\partial \sigma_f}{\partial \xi} = \Delta\sigma^{cr}. \tag{31}$$

with

$$\Delta\sigma^{cr} = \sigma_e^{cr} - \sigma_s^{cr} \tag{32}$$

σ_e^{cr} is the critical stress when transformation is finished. Martensite transformation is generally considered to be non-linear. To describe the non-linear transformation kinetics both exponential and trigonometrical functions have been employed (Tanaka, 1986; Brinson, 1993; Liang and Rogers, 1997). In this work polynomial functions of 5th-degree have been chosen to capture the non-linear hardening during both forward and reverse transformation. It is a numerically stable approach, and it is similar to the approach used in Abaqus (Rebelo, 2003), which this constitutive model is to be compared with. The polynomial function for the transformation flow stress can be written as

$$\sigma_f(\xi) = p_1^*\xi^5 + p_2^*\xi^4 + p_3^*\xi^3 + p_4^*\xi^2 + p_5^*\xi + p_6^* \tag{33}$$

The constants $p_1^*, p_2^*, p_3^*, p_4^*, p_5^*$ and p_6^* need to be determined through numerical fitting. The hardening rule becomes

$$\frac{\partial\sigma_f}{\partial\xi} = 5p_1^*\xi^4 + 4p_2^*\xi^3 + 3p_3^*\xi^2 + 2p_4^*\xi + p_5^*. \tag{34}$$

The change in flow stress can now be determined as

$$d\sigma_f = \frac{\partial\sigma_f}{\partial\xi}d\xi = (5p_1^*\xi^4 + 4p_2^*\xi^3 + 3p_3^*\xi^2 + 2p_4^*\xi + p_5^*)d\xi \tag{35}$$

The sign of $d\sigma_f$ is controlled by the sign of $d\xi$. It should be emphasized that the constants $p_i^*, i = 1-6$, are different for forward and reverse transformation.

In order to describe strain hardening during plastic deformation, an approach suggested by Aravas (1987) is used:

$$\frac{\sigma_f^{pl}}{\sigma_y} = \left(\frac{\sigma_f^{pl}}{\sigma_y} + \frac{3G}{\sigma_y}\varepsilon_{eq}^{pl}\right)^N. \tag{36}$$

where σ_y is the yield stress, $G = D/2(1+\nu)$ is the shear modulus and N is the hardening exponent. By rewriting Eq. (36) to

$$F = \frac{\sigma_f^{pl}}{\sigma_y} - \left(\frac{\sigma_f^{pl}}{\sigma_y} + \frac{3G}{\sigma_y}\varepsilon_{eq}^{pl}\right)^N = 0, \tag{37}$$

it is possible to establish the incremental change of the plastic flow stress as

$$d\sigma_f^{pl} = \frac{\frac{\partial F}{\partial\varepsilon_{eq}^{pl}}d\varepsilon_{eq}^{pl}}{\frac{\partial F}{\partial\sigma_f^{pl}}} \tag{38}$$

$$= \frac{\frac{\partial F}{\partial\varepsilon_{eq}^{pl}}}{\frac{\partial F}{\partial\sigma_f^{pl}}}\frac{\boldsymbol{\sigma} : \frac{\partial\Phi}{\partial\boldsymbol{\sigma}}}{(1-f)\sigma_f^{pl}}d\lambda \tag{39}$$

$$= h_{\sigma_f^{pl}}d\lambda, \tag{40}$$

with

$$\frac{\partial F}{\partial\varepsilon_{eq}^{pl}} = -\frac{3GN}{\sigma_y}\left(\frac{\sigma_f^{pl}}{\sigma_y} + \frac{3G}{\sigma_y}\varepsilon_{eq}^{pl}\right)^{N-1} \tag{41}$$

and

$$\frac{\partial F}{\partial\sigma_f^{pl}} = \frac{1 - N\left(\frac{\sigma_f^{pl}}{\sigma_y} + \frac{3G}{\sigma_y}\varepsilon_{eq}^{pl}\right)^{N-1}}{\sigma_y}. \tag{42}$$

2.4. Effect of non-constant elasticity modulus

To this point the effect of elastic mismatch has not been discussed. For some shape memory alloys (e.g. NiTi-alloys) the elasticity modulus for austenite can be as much as three times larger, than for martensite. Accordingly, accounting for the elastic mismatch in a constitutive model becomes important as it has a considerable effect on the overall behavior of the material.

Stress induced martensite firstly develops in an austenite matrix at locations that experience stress concentrations (e.g. in the vicinity of inclusions) (Brinson et al., 2004). Several small martensite islands may arise from these locations simultaneously and grow as the stress is increased. In order to get an average elasticity modulus during transformation some homogenization scheme is needed. Auricchio and Sacco (1997) suggest two schemes that they consider realistically can describe the evolution of the equivalent elasticity modulus during transformation. For a three-dimensional case a Mori–Tanaka scheme derived from the Eshelby inclusion problem is used, while for a one-dimensional case they found that the simpler Reuss scheme to be appropriate (Auricchio and Sacco, 1997). In this work a one-dimensional formulation is implemented to compare the constitutive model with uniaxially loaded unit-cells in Abaqus, and the Reuss scheme is chosen. Accordingly the equivalent elasticity modulus can be written as

$$D(\xi) = \frac{D_a}{1 + (\frac{D_a}{D_m} - 1)\xi}. \tag{43}$$

Subscript a and m denotes austenite and martensite, respectively. For details on the derivation of Eq. (43) please refer to the aforementioned work by Auricchio and Sacco (1997).

The most significant effect of the elastic mismatch is a difference between the total strain during forward and reverse transformation, respectively. In a previous work, (Yan et al., 2003) stated that the elastic strain contribution is near equal during both forward and reverse transformation, and argued that as a consequence the transformation length is different for the two cases. More specific: reverse transformation length is smaller than the forward transformation length. In our opinion, however, there is a significant difference in the elastic strain contribution during forward and reverse transformation. With this in mind, consider the schematic one-dimensional stress–strain curve in Fig. 1. It is assumed that $f_0 = 0$ for which case it can be shown that $\varepsilon_{eq}^{tr} = \varepsilon_{11}^{tr}$. Accordingly, after completed forward and reverse transformation $\varepsilon_{11}^{tr} = \epsilon_L^{for}$ and $\varepsilon_{11}^{tr} = \epsilon_L^{rev}$, respectively. From Fig. 1 it is obvious that

$$\varepsilon_{AB}^{el} + \varepsilon_{BC}^{el} + \varepsilon_{BC}^{tr} = \varepsilon_{CD}^{el} + \varepsilon_{DA}^{el} + \varepsilon_{DA}^{tr} \tag{44}$$

Now, let $\sigma_B = \sigma_s^{for}$, $\sigma_C = \sigma_e^{for}$, $\sigma_D = \sigma_s^{rev}$, $\sigma_A = \sigma_e^{rev}$, $\varepsilon_{BC} = \varepsilon_{BC}^{el} + \epsilon_L^{for}$ and $\varepsilon_{DA} = \varepsilon_{DA}^{el} + \epsilon_L^{rev}$. Rewriting Eq. (44) using Hooke's law yields

$$\frac{\sigma_s^{for} - \sigma_e^{rev}}{D_a} + \frac{\sigma_e^{for}}{D_m} - \frac{\sigma_s^{for}}{D_a} + \epsilon_L^{for} = \frac{\sigma_e^{for} - \sigma_s^{rev}}{D_m} + \frac{\sigma_s^{rev}}{D_m} - \frac{\sigma_e^{rev}}{D_a} + \epsilon_L^{rev} \tag{45}$$

$$\Rightarrow \epsilon_L^{rev} = \epsilon_L^{for} \tag{46}$$

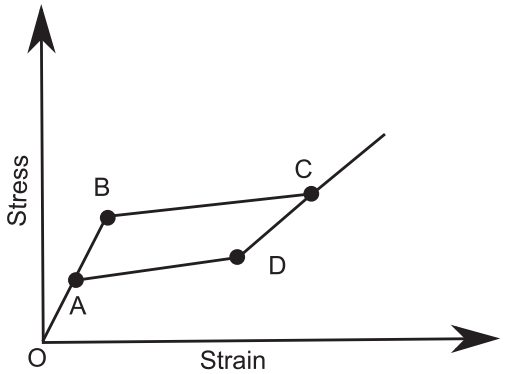

Fig. 1. Schematic stress–strain.

This shows that the forward and reverse transformation length is equal. ϵ_L^{for}, can be determined from mechanical testing (Brinson, 1993).

When the Gurson–Tvergaard–Needleman model is used with conventional materials, the effect of initial void volume fraction on the elasticity modulus is ignored. This can generally be accepted since the plastic strain is usually several orders larger than the elastic strain. However, when considering the superelastic behavior of shape memory alloys with non-constant elasticity modulus, the elastic strain and the transformation strain are almost of the same order. Therefore, particularly for larger void volume fractions, the effect of the initial void volume fraction on the elasticity modulus has to be accounted for. By considering elastic finite element analyses of axis-symmetric unit-cells (see Section 3 for finite element set-up) it is found that the effect of the initial void volume fraction on the elasticity modulus of austenite, D_a, can be written as

$$D_a^* = (1 + \alpha f_0) D_a. \tag{47}$$

where α is a constant. During phase transformation, void growth is relatively small so it is reasonable to assume that it does not significantly affect the elasticity modulus. Consequently it is assumed that Eq. (47) also holds for the case of a non-constant elasticity modulus. The equivalent elasticity modulus then becomes

$$D^*(f_0, \xi) = (1 + \alpha f_0) D(\xi). \tag{48}$$

Here $D(\xi)$ is expressed through Eq. (43).

Returning to the effect of elastic mismatch on the behavior of shape memory alloys: since the elasticity modulus changes during transformation, it can no longer be treated as a constant. As a consequence, Hooke's law must now be written as (assuming a one-dimensional stress state)

$$\sigma_{11} = \sigma_{11}(D^*, \varepsilon_{11}) = D^* \varepsilon_{11}^{el} \tag{49}$$

The change in stress may be written as

$$\begin{aligned} d\sigma_{11} &= \frac{\partial \sigma_{11}}{\partial \varepsilon_{11}^{el}} d\varepsilon_{11}^{el} + \frac{\partial \sigma_{11}}{\partial D^*} dD^* = D^* d\varepsilon_{11}^{el} + \varepsilon_{11}^{el} dD^* \\ &= D^*(d\varepsilon_{11} - d\varepsilon_{11}^{tr}) + \frac{\sigma_{11}}{D^*} dD^*. \end{aligned} \tag{50}$$

Since f_0 is constant, the change of the elasticity modulus during transformation can be written as

$$dD^* = \frac{\partial D^*}{\partial \xi} d\xi = -(1 + \alpha f_0) \frac{D_a D_m (D_a - D_m)}{[D_m(\xi - 1) - D_a \xi]^2} d\xi. \tag{51}$$

Employing the result in Eqs. (50) and (51) in conjunction with the consistency condition $d\Phi = 0$ for a one dimensional stress-state yields for the change in martensite volume fraction (not separating between forward and reverse transformation):

$$d\xi = \frac{\frac{\partial \Phi}{\partial \sigma_{11}} D^* d\varepsilon_{11}}{\frac{\partial \Phi}{\partial \sigma_{11}} D^* \frac{\partial \Phi}{\partial \sigma_{11}} \beta - \frac{\partial \Phi}{\partial \sigma_{11}} \frac{\sigma_{11}}{D^*} \frac{\partial D^*}{\partial \xi} - \frac{\partial \Phi}{\partial f} h_f \beta - \frac{\partial \Phi}{\partial \sigma_f} \frac{\partial \sigma_f}{\partial \xi}} \tag{52}$$

$$= h_\xi d\varepsilon_{11} \tag{53}$$

2.5. Material parameters β^{for} and β^{rev}

In order to determine the material parameter β^{for} we have to revisit Eq. (9) and perform an integration from transformation start to transformation finish. As transformation only can occur in the matrix of the material we assume that β^{for} and β^{rev} can be established for the case $f_0 = 0$, and be valid for all values of f_0. According to Eq. (8) the equivalent stress during forward transformation now becomes:

$$q = \sigma_f^{for} \tag{54}$$

Eq. (9) can then be written as (considering the 11-direction only)

$$d\varepsilon_{11}^{tr} = \beta^{for} d\xi \frac{\partial \Phi^{for}}{\partial \sigma_{11}} = \beta^{for} \frac{2}{\sigma_f^{for}(\xi)} d\xi \tag{55}$$

Definite integrals on both sides yield

$$\int_0^{\epsilon_L^{for}} d\varepsilon_{11}^{tr} = \beta^{for} \int_0^1 \frac{2}{\sigma_f^{for}} d\xi \Rightarrow \beta^{for} = \frac{\epsilon_L^{for}}{2 \int_0^1 \frac{1}{\sigma_f^{for}(\xi)} d\xi} \tag{56}$$

Similarly we get for reverse transformation

$$\beta^{rev} = \frac{\epsilon_L^{rev}}{2 \int_0^1 \frac{1}{\sigma_f^{rev}(\xi)} d\xi}. \tag{57}$$

Eqs. (56) and (57) show that β^{for} and β^{rev} depend on the hardening function used in the constitutive model. They are easily derived for non-hardening and linearly hardening materials, and can be written as

$$\beta^{for} = \frac{1}{2} \epsilon_L^{for} \sigma_s^{for}, \quad \beta^{rev} = \frac{1}{2} \epsilon_L^{rev} \sigma_s^{rev} \tag{58}$$

for a non-hardening material, and

$$\beta^{for} = \frac{\epsilon_L^{for}(\sigma_e^{for} - \sigma_s^{for})}{2 \ln\left(\frac{\sigma_e^{for}}{\sigma_s^{for}}\right)}, \quad \beta^{rev} = \frac{\epsilon_L^{rev}(\sigma_e^{rev} - \sigma_s^{rev})}{2 \ln\left(\frac{\sigma_e^{rev}}{\sigma_s^{rev}}\right)} \tag{59}$$

for a linearly hardening material, respectively. For the 5th-degree polynomial used as a non-linear hardening function in this work, β^{for} and β^{rev} are best determined through numerical integration.

3. Finite element analyses of axis-symmetric unit-cell models

In previous works the axis-symmetric void cell model has been employed to investigate the effect of micro-voids on ductile fracture in elasto-plastic materials (Koplik and Needleman, 1988; Pardoen and Hutchinson, 2000; Zhang et al., 2000). In this work a similar approach is adopted. Several unit-cell models with varying initial void volume fraction, f_0, are investigated. The finite element analyses will serve as a basis for verification of the proposed constitutive model, as well as a tool to investigate inherent effects of micro-voids on shape memory alloys. A sketch of the unit-cell model used in the finite element analyses is depicted in Fig. 2. To save computational time only a quarter of the unit-cell is modeled and it consists of 288 linear 4-node axis-symmetric elements. Attempts were made with quadratic 8-node axis-symmetric elements, however, convergence issues lead to unsatisfactory deformation levels. The unit-cell has a total height $2L_y$ and a radius L_x. The ellipsoidal micro-voids have radii r_y and r_x, in the axial direction and radial direction of the unit-cell, respectively. In Fig. 2 P_y and P_x denotes the load in the axial and radial direction, respectively. The micro-void geometrical characteristics can be represented by initial void volume fraction and the aspect ratio by the equations

$$f_0 = \frac{2 r_{y0} r_{x0}^2}{3 L_{y0} L_{x0}^2}; \quad h_0 = \frac{r_{y0}}{r_{x0}} \tag{60}$$

where subscript "0" denotes initial value. This approach is limited by the cases when $h_0 \to 0$ and $h_0 \to \infty$ (Pardoen and Hutchinson, 2000). In the current study, only cases with $h_0 = 1$ have been investigated, i.e. spherical micro-voids.

The mesoscopic logarithmic principal strains, E_x and E_y, and the effective strain, E_e, are given by

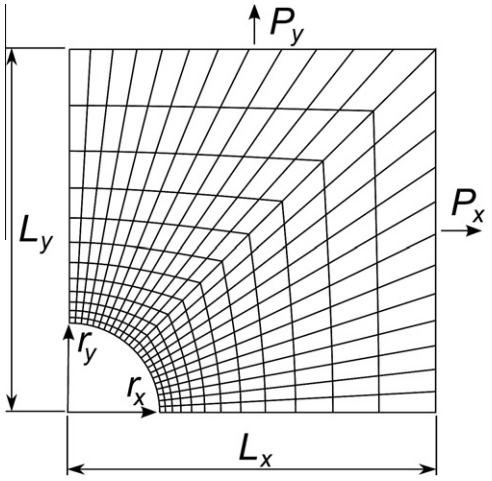

Fig. 2. Unit-cell model used in the finite element simulations.

$$E_x = ln\left(\frac{L_x}{L_{x0}}\right); \quad E_y = ln\left(\frac{L_y}{L_{y0}}\right); \quad E_e = \frac{2}{3}|E_y - E_x|, \tag{61}$$

while the mesoscopic principal stresses, Σ_y and Σ_x, and the effective stress, Σ_e are calculated as

$$\Sigma_y = \frac{P_y}{A}; \quad \Sigma_x = \Sigma_y \rho; \quad \Sigma_e = |\Sigma_y(1-\rho)|. \tag{62}$$

where $A = \pi L_x^2$ is the current area, and ρ is the stress proportionality factor. The hydrostatic stress, Σ_h, and the stress triaxiality, T, are given by

$$\Sigma_h = \frac{1}{3}\Sigma_y(1+2\rho); \quad T = \frac{\Sigma_h}{\Sigma_e} = \frac{1}{3}\left[\frac{1+2\rho}{1-\rho}\right]. \tag{63}$$

In order to have the possibility to impose a triaxial stress state, a multi-point constraint user subroutine, MPC, has been used; two linear springs, A and B, are added to the axis-symmetric model – one at the top left corner and one at the bottom right corner. Through the load proportionality condition it is possible to establish a relationship between the deformation in spring A and spring B (Søvik, 1996):

Table 1
Material parameters needed in Rebelo's model, and used in the finite element simulations.

Parameter	Value	Description
D_A [MPa]	47,000	Elasticity modulus for austenite
D_M [MPa]	15,667	Elasticity modulus for martensite
ν_A, ν_M	0.33	Poisson ratio for austenite and martensite
σ_s^{for} [MPa]	351	Critical stress for start of forw. trans.
σ_e^{for} [MPa]	422	Critical stress for end of forw. trans.
σ_s^{rev} [MPa]	250	Critical stress for start of rev. trans.
σ_e^{rev} [MPa]	175	Critical stress for end of rev. trans.
ϵ^L	0.026	Transformation length
$\varepsilon_1^{pl}, \sigma_1^{pl} \cdots \varepsilon_N^{pl}, \sigma_N^{pl}$		Stress–strain pairs during plastic deformation

Table 2
Constants used in polynomial hardening functions.

	p_1	p_2	p_3	p_4	p_5
Forw. trans.	1.75	−4.51	4.40	−2.01	0.56
Rev. trans.	8.03	−22.5	23.6	−11.6	2.90

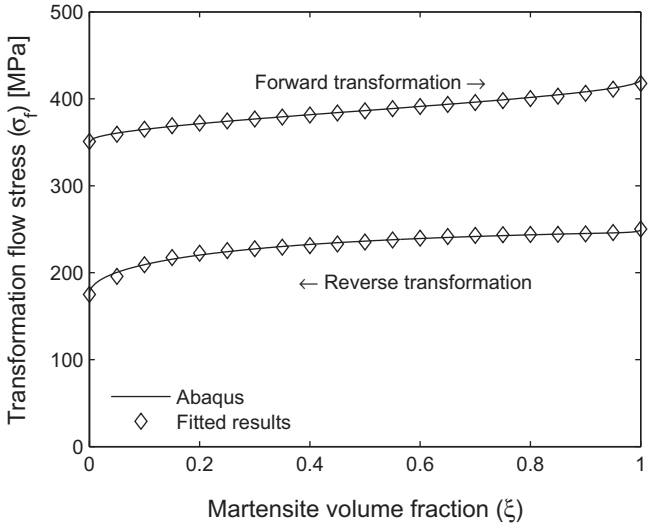

Fig. 3. Comparison of ξ-σ_f curves from Abaqus and the new constitutive model for $f_0 = 0$.

$$u_x^a = u_x^b + 2\rho\frac{k_A}{k_B}\frac{(u_y^d - u_y^c)(L_{y0} + u_y^c)}{(L_{x0} + u_x^b)} \tag{64}$$

where $u_x^a, u_x^b, u_y^c, u_y^d, k_A$ and k_B are displacements and stiffnesses in springs A and B, respectively. During analyses in Abaqus, displacement u_y^d is applied, and displacement u_x^a follows from Eq. (64) which is included in the MPC. As the constitutive model to be compared with the finite element analyses is only implemented for a one dimensional stress state, all simulations where conducted with a load proportionality factor, $\rho = 0$, i.e. $T = 0.33$.

The constitutive model is developed and implemented in the commercial finite element software Abaqus at SIMULIA/west by

Table 3
β^{for} and β^{rev} calculated for different types of hardening.

	No hardening	Linear hardening	Non-linear hardening
β^{for}[MPa]	4.56	5.01	5.02
β^{rev}[MPa]	3.25	2.73	2.99

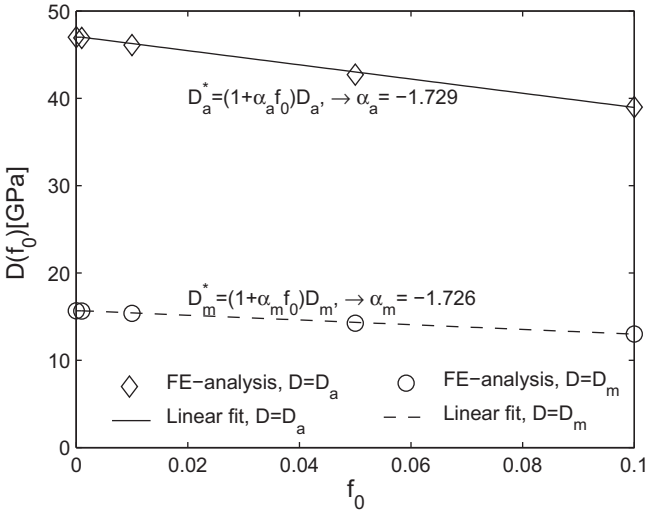

Fig. 4. Comparison of the effect of initial void volume fraction on the average elasticity modulus for two different cases.

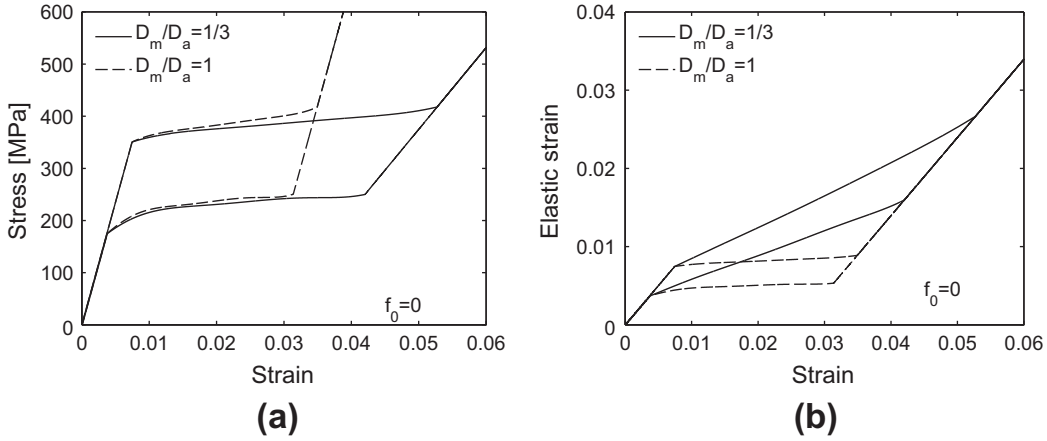

Fig. 5. Results showing the effect of elastic mismatch on the (a) stress–strain relations, (b) the elastic strain.

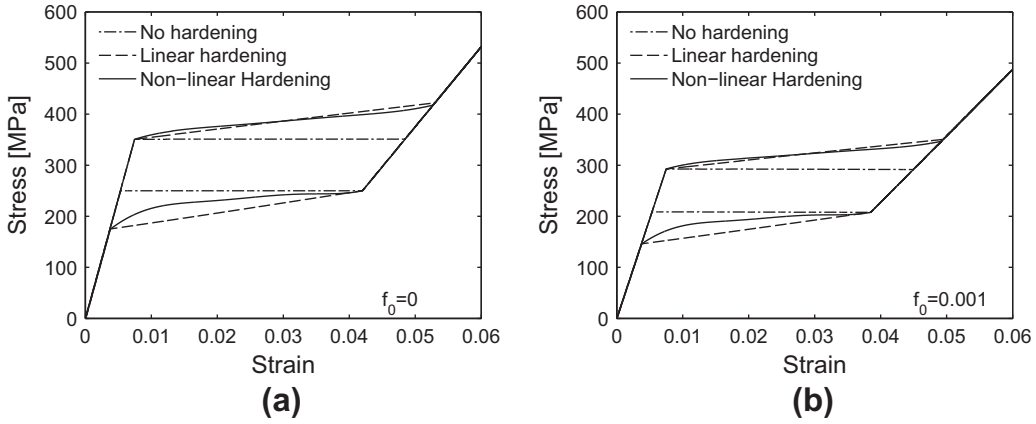

Fig. 6. Stress–strain curves comparing the effect of different hardening types when initial void-volume fraction is (a) $f_0 = 0$ and (b) $f_0 = 0.1$.

Rebelo (2003). It is an extension of Auricchio's model that accounts for plastic deformations, and is readily available as a user subroutine, UMAT, in Abaqus (SIMULIA, 2010). A description of the model can be found in a paper by Rebelo (2003). The material data needed for Rebelo's model, and used in the finite element simulations are presented in Table 1.

As the problem at hand is of a highly non-linear nature and convergence becomes difficult at large deformation levels, selected convergence criteria were relaxed to be able to reach satisfactory deformation levels (Olsen et al., 2011).

3.1. Fitting material parameters in the new constitutive model

All material parameters presented in Table 1 which are originally used in accordance with the shape memory alloy model used in Abaqus are also valid for the new constitutive model presented in this work. In addition, constants $p_i^*, i = 1-6$ from Eq. (34), α, β^{for} and β^{rev} need to be calculated.

By evaluating Eq. (34) at $\xi = 0$ it is obvious that $p_6^{*for} = \sigma_s^{for}$ and $p_6^{*rev} = \sigma_e^{rev}$. This allows us to rewrite Eq. (34) on the form

$$\sigma_f^{for}(\xi) = \sigma_s^{for}\left(p_1^{for}\xi^5 + p_2^{for}\xi^4 + p_3^{for}\xi^3 + p_4^{for}\xi^2 + p_5^{for}\xi + 1\right) \tag{65}$$

$$\sigma_f^{rev}(\xi) = \sigma_e^{rev}\left(p_1^{rev}\xi^5 + p_2^{rev}\xi^4 + p_3^{rev}\xi^3 + p_4^{rev}\xi^2 + p_5^{rev}\xi + 1\right), \tag{66}$$

for forward and reverse transformation, respectively. The remaining constants have been determined from the finite element results through a linear least square curve fitting and are presented in Table 2. A comparison between the finite element analyses and the fitted new constitutive model is shown in a ξ-σ_f curve in Fig. 3. The figure shows a full transformation hysteresis from the finite element analysis for a unit-cell with $f_0 = 0$ and Eqs. (65) and (66) for forward and reverse transformation, respectively.

The material parameters β^{for} and β^{rev} are calculated by using the material parameters presented in Table 1 in Eqs. (58) and (59) for the cases of no hardening and linear hardening, respectively. For the case of non-linear hardening the same material parameters have been calculated by performing a numerical integration of Eqs. (56) and (57). The calculated values of β^{for} and β^{rev} are presented for all types of hardening in Table 3.

As mentioned, the effect of initial void volume fraction on the average elasticity modulus is accounted for in the new constitutive model. It is assumed that the constant α in Eq. (47) is the same for all initial values of the elasticity modulus, D. In order to verify this, elastic finite element analyses have been conducted for unit-cells with void volume fractions in the range $f_0 = 0 - 0.1$ for two cases: one with $D = D_a$ and one with $D = D_m$. Fig. 4 shows the elasticity moduli calculated from the numerical analyses, and a linear fit which is used to determine α. It is found that the case of $D = D_a$, the constant is $\alpha_a = -1.729$ and for the case $D = D_m$ it is $\alpha_m = -1.726$. This gives a deviation of 0.16% which is considered accurate enough to assume that α remains constant during transformation eventhough the elasticity modulus changes.

The last constants in this constitutive model that need to be determined, are k_1 and k_2. If $k_1 = k_2 = 1$, the transformation potential is similar to the original Gurson formulation. For the cases

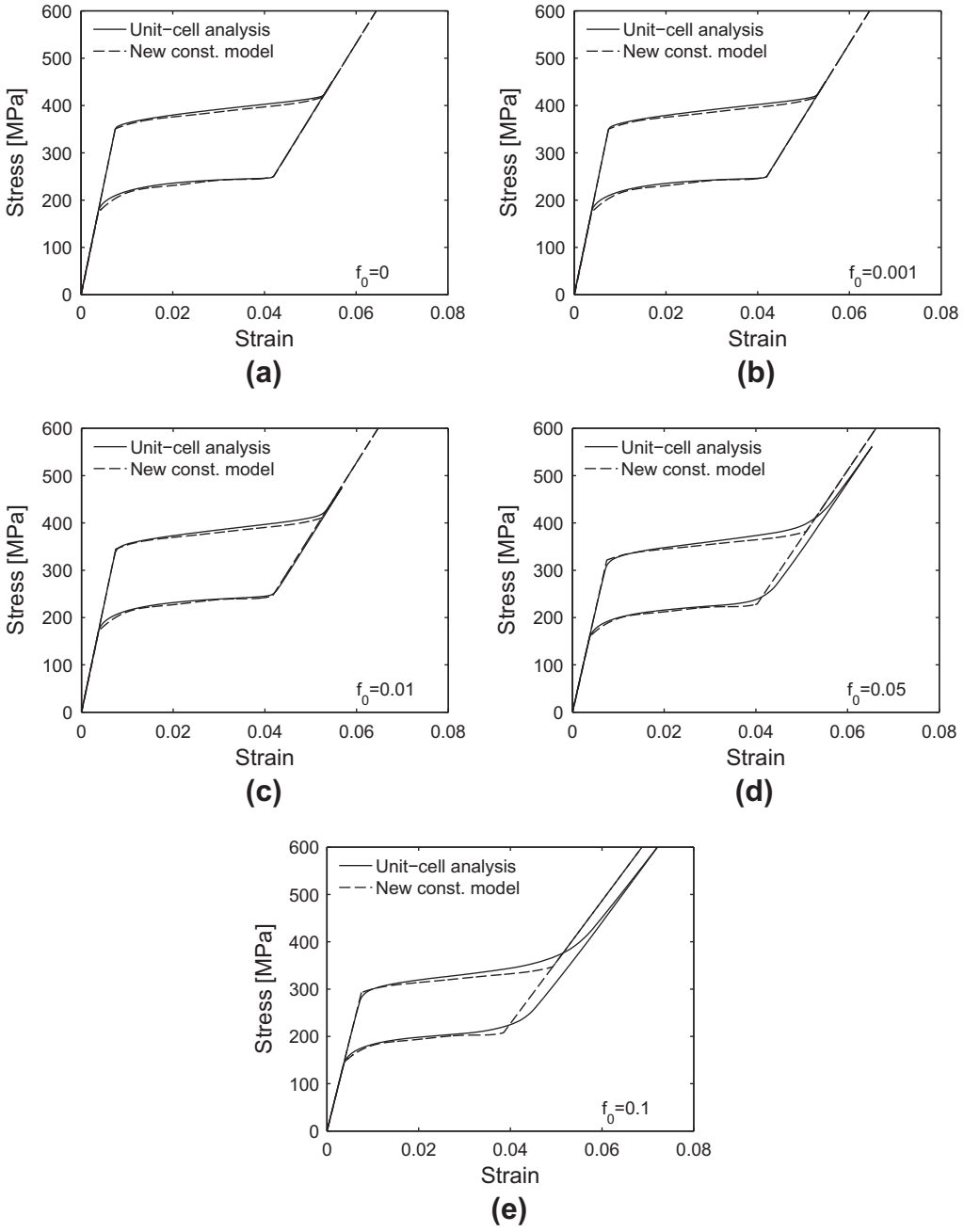

Fig. 7. Superelastic stress–strain hystereses comparing between results from finite element unit-cell analyses and the new constitutive model when initial void-volume fraction is (a) $f_0 = 0$, (b) $f_0 = 0.001$, (c) $f_0 = 0.01$, (d) $f_0 = 0.05$ and (e) $f_0 = 0.1$.

investigated herein it is found that stress levels calculated with the new constitutive model are more accurately described if the constants k_1 and k_2 are set to 1.5 and 1, respectively.

4. Results and discussion

4.1. Effect of transformation hardening and elastic mismatch

It has previously in this paper been argued that the behavior of shape memory alloys is considerably affected if a non-constant elasticity modulus is accounted for. To quantify this effect, a case where $D_m = D_a$ is compared with a case where $D_m = \frac{1}{3}D_a$. For both cases the initial void volume fraction is set to $f_0 = 0$. Fig. 5(a) shows the stress–strain curves, and the main difference is that the transformation plateaus is much larger when $D_m = \frac{1}{3}D_a$ than for the case when $D_m = D_a$. This effect can be exclusively attributed to an increase of the elastic strains during transformation. In Fig. 5(b) the elastic strain in the axial direction is compared for the two cases, and when a non-constant elasticity modulus is considered, the elastic strain contribution during both forward and reverse transformation is more than three times higher than when a constant elasticity modulus is considered.

The proposed constitutive model has been developed so that any desired transformation hardening rule can be used. Changing the hardening rule will ultimately affect the stress in the material during transformation, and should not affect the length of the transformation plateaus. It is noted that to ensure this, the material

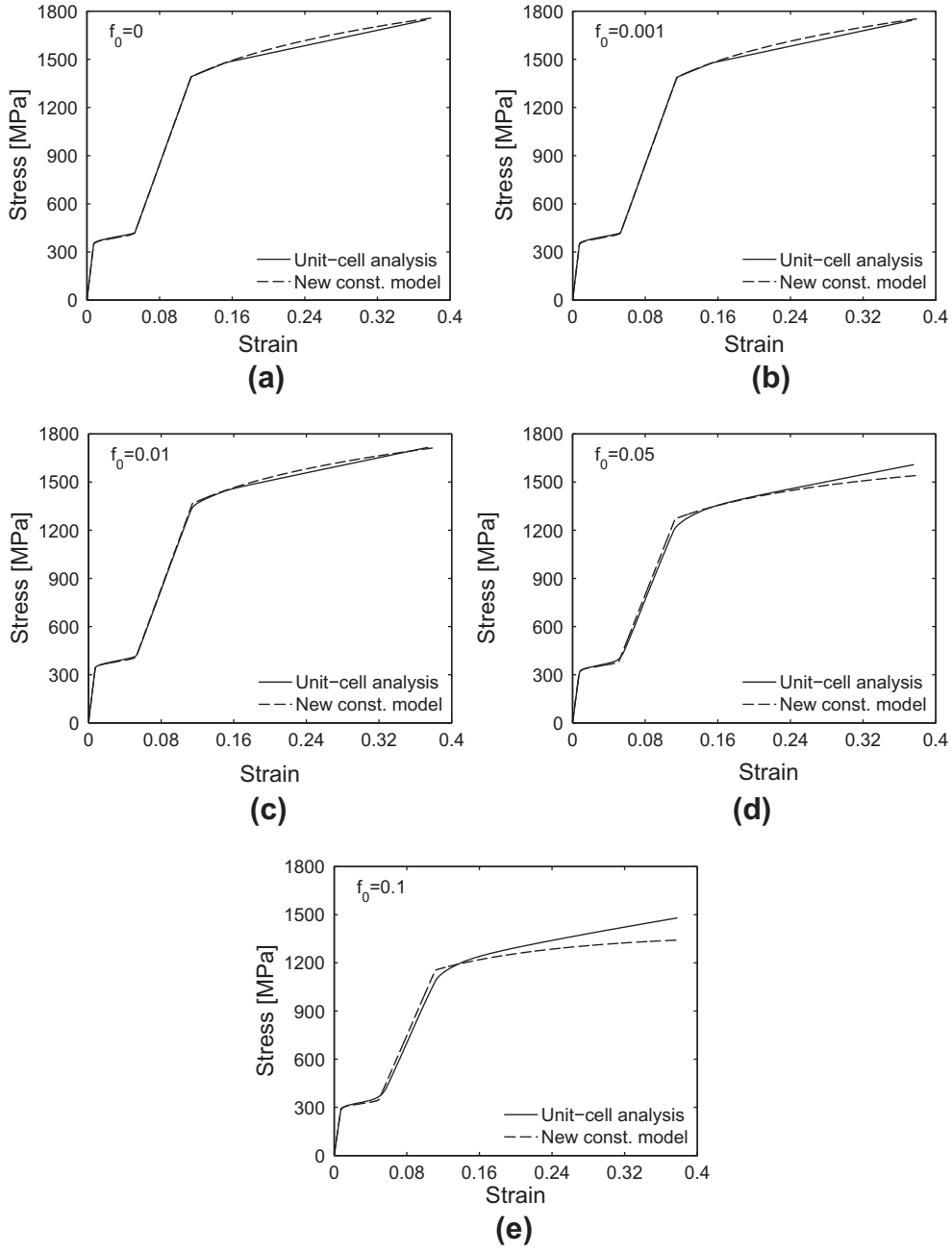

Fig. 8. Superelastic–plastic stress–strain curves comparing between results from finite element unit-cell analyses and the new constitutive model when initial void-volume fraction is (a) $f_0 = 0$, (b) $f_0 = 0.001$, (c) $f_0 = 0.01$, (d) $f_0 = 0.05$ and (e) $f_0 = 0.1$.

parameters β^{for} and β^{rev}, which indirectly controls the length of transformation plateau, need to be adapted to whatever hardening rule is chosen (refer Section 2.5). Fig. 6 shows the stress strain curves for materials with $f_0 = 0$ and $f_0 = 0.1$ where the effect of no hardening, linear hardening and non-linear hardening is compared. Here non-linear hardening is represented through the 5th-degree polynomials presented in Section 2.3. The linear and non-linear hardening rules are both able to well capture all the critical stresses for transformation start and finish, while the case with no hardening exhibit a good fit for the critical stress for onset of transformation only. For the latter case there is actually a slight decrease in the stress during forward transformation and a corresponding increase during reverse transformation. However, most important is that there is no discrepancy when it comes to length of the transformation plateaus for any of the three cases. This shows that the proposed model has the potential to function well for any kind of transformation hardening rule.

4.2. Comparison of finite element analyses and the new constitutive model

In Fig. 7 stress–strain hystereses are shown for five different initial void volume fractions, ranging from $f_0 = 0$ to $f_0 = 0.1$. The figure presents results from both finite element unit-cell analyses and the new constitutive model. All analyses are conducted with uni-axial loading, and for the unit-cells maximum strain before unloading, is set to be when the response is close to linear elastic. The results show that for small void volume fractions, f_0 = 0–0.01, the new constitutive model capture well the stress–strain response of the unit-cells. For larger void volume fractions, f_0 = 0.05–0.1, the elastic

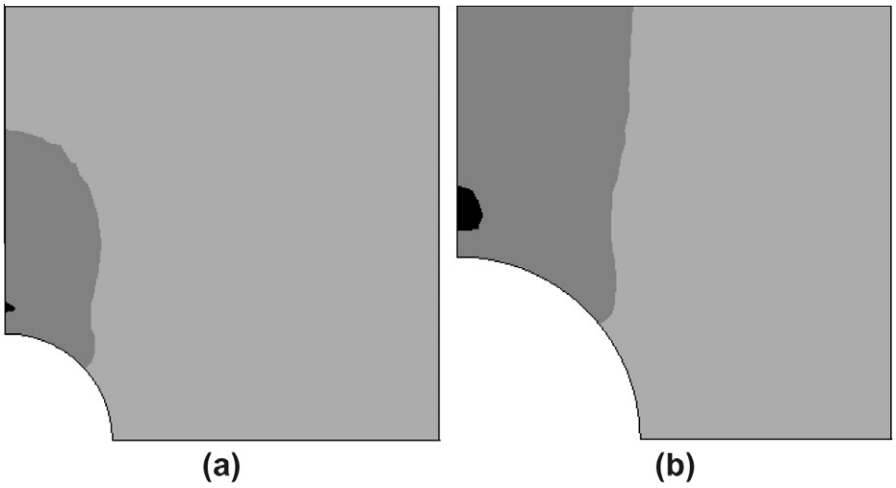

Fig. 9. The three phases coexisting at $E_x = 0.15$ in a unit-cell with (a) $f_0 = 0.01$ (b) $f_0 = 0.05$. Phase transformation, elastic deformation and plastic deformation are indicated by black, gray and light gray colors, respectively.

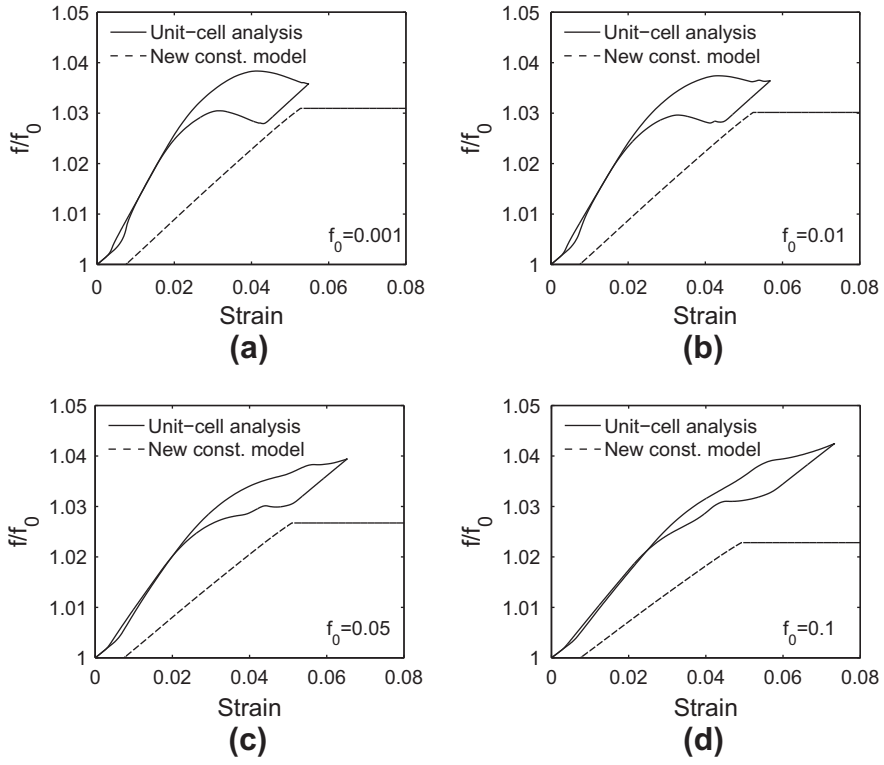

Fig. 10. Curves comparing void-growth as a function of strain between results from finite element unit-cell analyses and the new constitutive model, for one superelastic cycle, when initial void-volume fraction is (a) $f_0 = 0.001$, (b) $f_0 = 0.01$, (c) $f_0 = 0.05$ and (d) $f_0 = 0.1$.

deformation prior to, and the onset of, forward transformation are well described by the new constitutive model. However, as phase transformation comes closer to completion ($\varepsilon_{11} \approx 0.03$), the stress recorded from the unit-cell models increase faster. Also, it can be seen that the transformation plateau is longer and not as clearly defined as it is for the new constitutive model.

The stress field in a unit-cell with micro-void is highly inhomogeneous, and a stress concentration will arise close to the micro-void at the base of the unit-cell. As the phase transformation is stress driven, the martensite volume fraction exhibits the same inhomogeneous behavior. The consequence is that the mechanical properties will differ within the matrix of the unit-cell, with parts behaving elastically after completed transformation while other parts still undergo phase transformation. In the proposed constitutive model, it is assumed that phase transformation is homogeneous in the matrix with a clearly defined start and finish. It does not capture the inhomogeneous stress field in the material. Consequently the stress–strain response will deviate somewhat from that of the unit-cells with larger void volume fractions.

Stress–strain curves exhibiting superelastic–plastic response are shown in Fig. 8 for the aforementioned void volume fraction range. As with the superelastic hystereses, the proposed constitutive model is also capable of well describing the elastic–plastic behavior subsequent to forward phase transformation for the smaller void

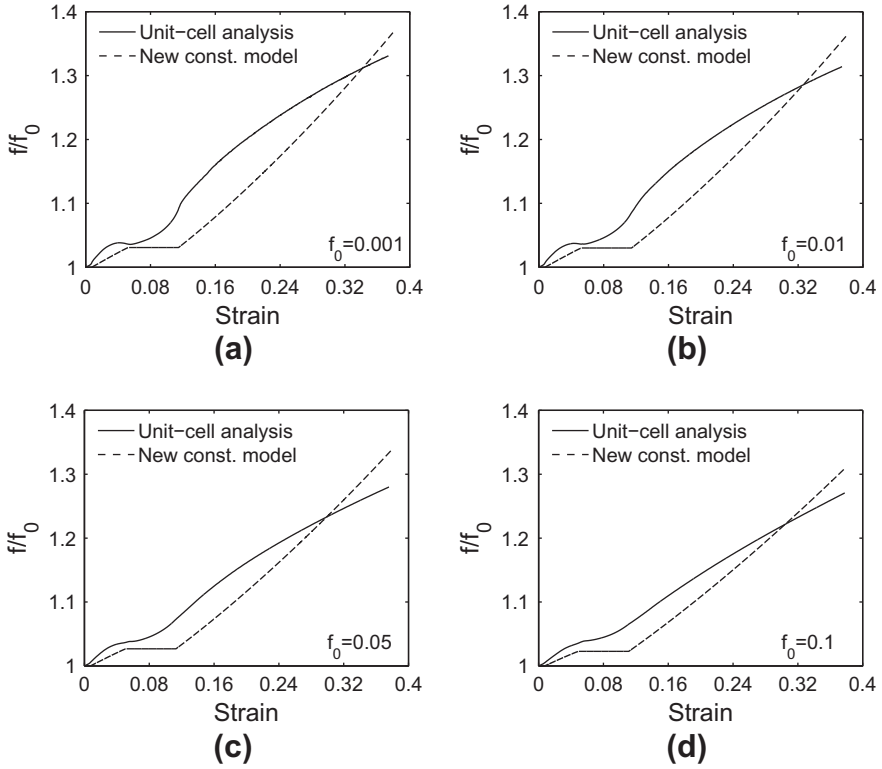

Fig. 11. Curves comparing void-growth as a function of strain between results from finite element unit-cell analyses and the new constitutive model, for forward transformation and subsequent plastic deformation, when initial void-volume fraction is (a) $f_0 = 0.001$, (b) $f_0 = 0.01$, (c) $f_0 = 0.05$ and (d) $f_0 = 0.1$.

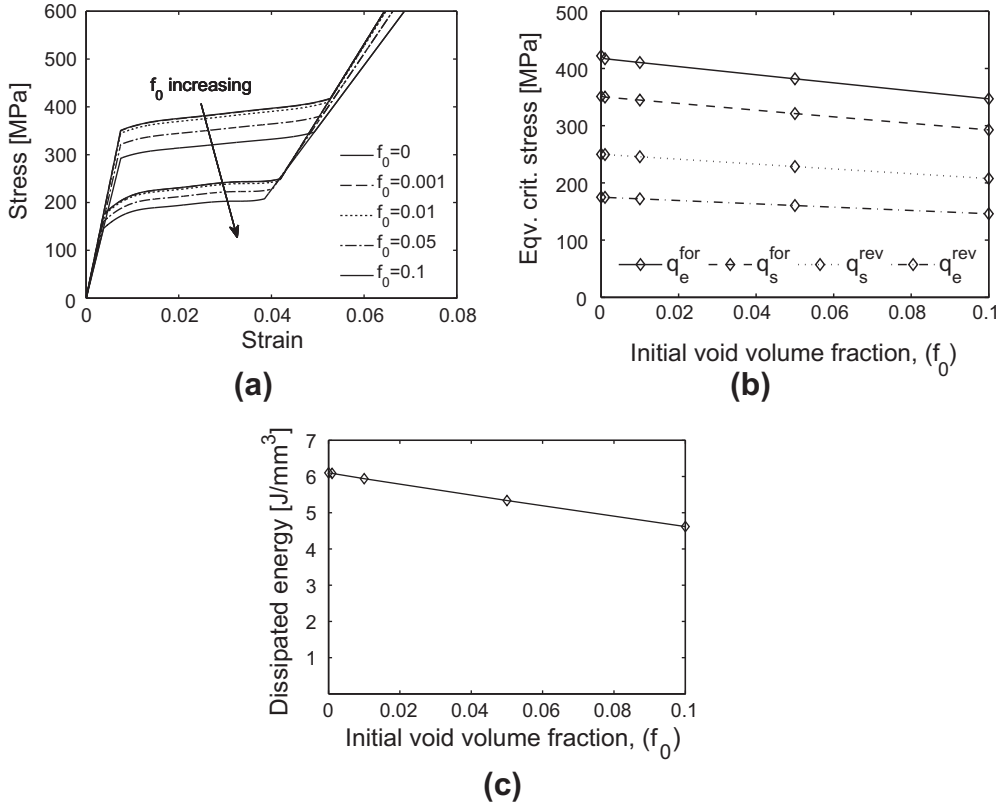

Fig. 12. Results showing the effect of micro-voids on (a) stress–strain relations, (b) the equivalent critical stress and (c) the dissipated energy after a full superelastic cycle.

volume fractions ($f_0 < 0.05$). However, for the larger void volume fractions ($f_0 \geqslant 0.05$) there is a significant discrepancy between the unit-cell analyses and the new constitutive model. For the case of $f_0 = 0.05$ there is a relatively good fit up to $\varepsilon_{11} \approx 0.24$ before the

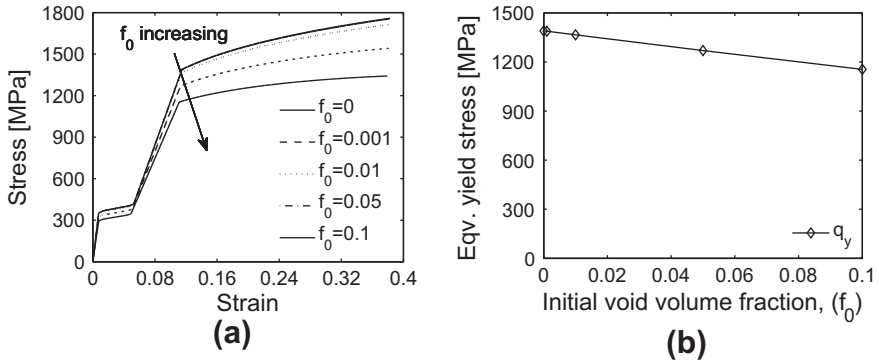

Fig. 13. Results showing the effect of micro-voids on (a) superelastic–plastic stress–strain relations, (b) the equivalent yield stress.

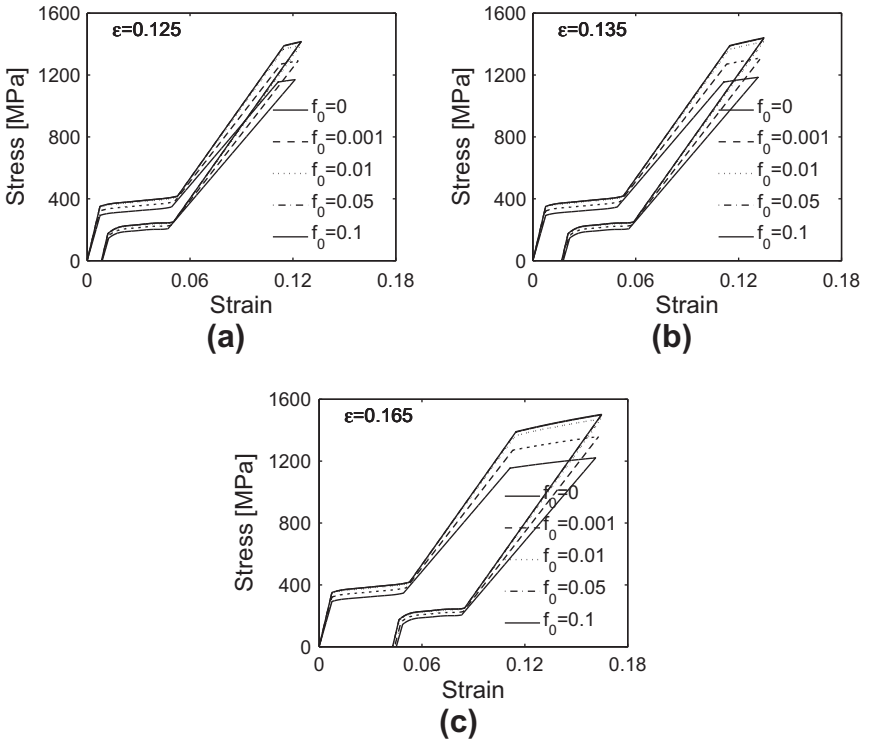

Fig. 14. Results showing the effect of micro-voids on (a) stress–strain relations, (b) the equivalent critical stress and (c) the dissipated energy after a full superelastic cycle.

curves start to deviate. When $f_0 = 0.1$ the proposed model is able to predict the average yield stress (onset of plastic deformation), but the stress is significantly lower for our model than the unit-cell analysis as the plastic deformation continues. Again, the reason for the difference in the results for larger void volume fractions can be explained by the assumption of a homogeneous stress field within the matrix of the material. In the unit-cells, the matrix essentially consists of three different materials after plastic deformation is initiated: elastic deformation, phase transformation and plastic deformation coexist. This is shown in Fig. 9 where a comparison between a unit-cell with $f_0 = 0.01$ and a unit-cell with $f_0 = 0.05$ is made at a strain of $E_x = 0.15$. The parts of the unit-cell which experience phase transformation, elastic deformation subsequent to phase transformation and plastic deformation are indicated by black, gray and light gray colors, respectively. For the larger void volume fractions the inhomogeneity effect is much more pronounced as the volume of the material experiencing non-plastic deformation is considerably larger than for the smaller void volume fractions. As parts of the unit-cell experience elastic deformation the average stress will become higher than for the proposed constitutive model which assumes pure plastic deformation at this stage. It should be noted that the different phases are represented trough the equivalent von Mises stress, i.e. phase transformation occurs when the Mises stress is lower than σ_e^{for}, plastic deformation occurs when the Mises stress is higher than σ_y and elastic deformation occur in between these values.

From Fig. 10 it can be seen that there is a considerable discrepancy between void-growth in the unit-cells and that calculated by the proposed constitutive model. Void-growth is in this work defined as an increase in the *void volume fraction*. In the proposed model it is assumed that void-growth due to elastic strain is negligible, an approach commonly used with GTN-like constitutive models, and that it is only affected by the volumetric transformation strain. By examining the void-growth curves extracted from the finite element unit-cell analyses it is obvious that for a superelastic material, the elastic strain is of significance for the degree of void-growth. For strain up to onset of transformation start ($\varepsilon_{11} \approx 0.007$), the unit-cell analyses all exhibit some degree of

void-growth. Also, when unloading the unit-cells a negative void-growth can be observed that is directly associated with elastic deformation (e.g. for the unit-cell with $f_0 = 0.001$ this can be seen when unloading from strain $\varepsilon_{11} = 0.0548$ to $\varepsilon_{11} = 0.0485$). For the unit-cells, when the deformation is dominated by phase transformation, the void-growth attains a close to linear response until a certain degree of fully transformed material is present. In the proposed model, the influence of void-growth on the superelastic behavior has been investigated by performing analyses at which $df = 0$ (not shown here). The results showed that there is no significant effect on the superelastic stress–strain relations for any of the cases investigated herein.

An interesting feature can be observed in Fig. 10(a) and Fig. 10(b) at a certain strain level ($\varepsilon_{11} \approx 0.04$) the total void volume fraction peaks, and subsequently decreases as the strain increases. Reduction of the void volume fraction occurs for the smaller micro-voids because the volume of the matrix increases more than the void volume. The elasticity modulus changes during transformation which leads to a considerable increase of the elastic strains in the matrix. Void-growth is mainly driven by inelastic strains. At the start of phase transformation, the transformation strains increase faster than the elastic strains, and consequently promotes void-growth. In the unit-cells, after a certain deformation level, the micro-voids gradually becomes engulfed by a fully transformed volume which is now behaving purely elastic. This elastic deformation will somewhat hinder increase of the void volume, while at the same time the matrix experience an increase of the elastic strains. Accordingly, the matrix volume increases faster than the void volume thus causing a decrease in the void volume fraction. This effect is not present for the larger void-volume fractions. It is noted that the void volume fractions calculated from the unit-cells exhibit an increase of $\sim 4\%$ before unloading for all the cases investigated herein.

In Fig. 11 the void-growth is shown for analyses from both the unit-cell model and the new constitutive model. The unit-cell analyses consistently predicts a higher void volume fraction than the proposed constitutive model for strains, $\varepsilon_{11} < 0.3$. However, for strains, $\varepsilon_{11} > 0.3$ the void-growth is higher for the new constitutive model.

4.3. Effect of micro-voids on stress–strain relations

The most pronounced effect of introducing micro-voids in the material is that with increasing initial void volume fraction, the average stress level is overall reduced. In Fig. 12(a) it can be seen that there is a downward shift of the stress–strain hystereses as the initial void volume fraction increases. This means that for a material with micro-voids, transformation will be induced, and completed, at a lower stress than a homogeneous material. Fig. 12(b) shows the equivalent critical stresses at $\xi = 0$ and $\xi = 1$, for both forward (q_s^{for}, q_s^{rev}) and reverse (q_e^{for}, q_e^{rev}) transformation when f_0 is increased from 0 to 0.1. For the same cases the results show that there is a linear relation between the equivalent critical stresses and the initial void volume fraction, and that $q_s^{for}, q_e^{for}, q_s^{rev}$ and q_e^{rev} are reduced by 20%, 21.6%, 20.4% and 19.9%, respectively. A similar observation can be made for the average yield stress (see Fig. 13): there is a 20% reduction when the void volume fraction is increased from $f_0 = 0$ to $f_0 = 0.1$.

Another effect attributed to the introduction of micro-voids that is not as easily observed from the stress–strain curves, is a narrowing of the hystereses as the initial void volume fraction increases. This effect is best measured by calculating the energy dissipated after a complete superelastic cycle. The dissipated energy is shown as a function of initial void volume fraction in Fig. 12(c). Approximately 24% less energy is dissipated when $f_0 = 0.1$ than for the case where $f_0 = 0$.

If plastic deformation occurs in a superelasic shape memory alloy, the ability for the material to completely regain its shape after unloading is reduced. In Fig. 14 stress–strain curves are shown for three different cases of plastic deformation. The total strain was chosen so that the plastic strain would amount to approximately 0.01, 0.02 and 0.05 for the different cases. It is interesting to observe that the initial void volume fraction has an increasing effect on the residual strain as the plastic strain is increased. When the plastic strain is approximately 0.01 there is almost no difference between residual strains for the various void volume fractions. However, if the plastic strain is increased to 0.05 the residual strain is approximately 4.5% larger when $f_0 = 0.1$, compared to the case when $f_0 = 0$.

5. Conclusions

In this work a new constitutive model has been proposed for shape memory alloys. The model is based on the Gurson–Tvergaard–Needleman model for elastic–plastic materials containing micro-voids and is modified to account for the superelastic–plastic behavior found in shape memory alloys. A one dimensional implementation using a forward Euler integrations scheme has been conducted.

Analyses from uniaxially loaded axis-symmetric unit-cells have been used to validate the model, and it is able to well replicate the stress–strain results from the finite element analyses for smaller void volume fractions ($f_0 < 0.05$). For void volume fractions $f_0 \geqslant 0.05$, however, there is a discrepancy between the finite element results and the results from the new constitutive model. The reason is that the proposed model does not account for the considerable inhomogeneous stress field that arise within the unit-cell matrix, which consists of three different phases.

Comparing results for different void volume fractions show that introducing micro-voids lowers the average stress level, and that both phase transformation and plastic yielding occur at considerably lower stress than for a homogeneous material. In addition, it is found that the superelastic stress–strain hystereses becomes narrower with increasing void volume fraction, i.e. the amount of energy dissipated during a stress–strain cycle is reduced.

References

Aravas, N., 1987. On the numerical integration of a class of pressure-dependent plasticity models. International Journal for Numerical Methods in Engineering 24 (7), 1395–1416.

Auricchio, F., Sacco, E., 1997. A one-dimensional model for superelastic shape-memory alloys with different elastic properties between austenite and martensite. International Journal of Non-Linear Mechanics 32 (6), 1101–1114.

Auricchio, F., Taylor, R.L., 1997. Shape-memory alloys: modelling and numerical simulations of the finite-strain superelastic behavior. Computer Methods in Applied Mechanics and Engineering 143 (1–2), 175–194.

Brinson, L., 1993. One-dimensional constitutive behavior of shape memory alloys: Thermomechanical derivation with non-constant material functions and redefined martensite internal variable. Journal of Intelligent Material Systems and Structures 4 (2), 229–242.

Brinson, L.C., Schmidt, I., Lammering, R., 2004. Stress-induced transformation behavior of a polycrystalline NiTi shape memory alloy: micro and macromechanical investigations via in situ optical microscopy. Journal of the Mechanics and Physics of Solids 52 (7), 1549–1571.

Chen, J.H., Sun, W., Wang, G.Z., 2005. Investigation on the fracture behavior of shape memory alloy niti. Metallurgical and Materials Transactions A: Physical Metallurgy and Materials Science 36 (4), 941–955.

Entchev, P.B., Lagoudas, D.C., 2002. Modeling porous shape memory alloys using micromechanical averaging techniques. Mechanics of Materials 34 (1), 1–24.

Entchev, P.B., Lagoudas, D.C., 2004. Modeling of transformation-induced plasticity and its effect on the behavior of porous shape memory alloys. Part II: Porous sma response. Mechanics of Materials 36 (9), 893–913.

Funakubo, H., 1987. Shape Memory Alloys. Precision and Robotics, 1. Gordon and Breach Science Publishers.

Gall, K., Yang, N., Sehitoglu, H., Chumlyakov, Y.I., 2001. Fracture of precipitated NiTi shape memory alloys. International Journal of Fracture 109 (2), 189–207.

Gollerthan, S., Herberg, D., Baruj, A., Eggeler, G., 2008. Compact tension testing of martensitic/pseudoplastic NiTi shape memory alloys. Materials Science and Engineering A 481–482 (1–2 C), 156–159.

Gurson, A.L., 1977. Continuum theory of ductile rupture by void nucleation and growth: Part 1 – Yield criteria and flow rules for porous ductile media. Transactions of the ASME Journal of Engineering Materials and Technology Series H 99 (1), 2–15.

Koplik, J., Needleman, A., 1988. Void growth and coalescence in porous plastic solids. International Journal of Solids and Structures 24 (8), 835–853.

Lagoudas, D.C., Entchev, P.B., 2004. Modeling of transformation-induced plasticity and its effect on the behavior of porous shape memory alloys. Part I: Constitutive model for fully dense mass. Mechanics of Materials 36 (9), 865–892.

Liang, C., Rogers, C.A., 1997. One-dimensional thermomechanical constitutive relations for shape memory materials. Journal of Intelligent Material Systems And Structures 8 (4), 285–302 (reprinted from Journal of Intelligent Material Systems and Structures, vol. 1, pp. 207–234, 1990).

Lubliner, J., Auricchio, F., 1996. Generalized plasticity and shape-memory alloys. International Journal of Solids and Structures 33 (7), 991–1003.

McKelvey, A.L., Ritchie, R.O., 2001. Fatigue-crack growth behavior in the superelastic and shape-memory alloy nitinol. Metallurgical and Materials Transactions A – Physical Metallurgy and Materials Science 32 (3A), 731–743.

Nemat-Nasser, S., Su, Y., Guo, W.G., Isaacs, J., 2005. Experimental characterization and micromechanical modeling of superelastic response of a porous NiTi shape-memory alloy. Journal of the Mechanics and Physics of Solids 53 (10), 2320–2346.

Olsen, J.S., Zhang, Z.L., Hals, J.K., Lu, H., 2011. Effect of notches on the behavior of superelastic round-bar niti-specimens. Smart Materials and Structures 20 (2).

Otsuka, K., Ren, X., 2005. Physical metallurgy of ti–ni**-based shape memory alloys. Progress in Materials Science 50 (5), 511–678.

Panico, M., Brinson, L.C., 2008. Computational modeling of porous shape memory alloys. International Journal of Solids and Structures 45 (21), 5613–5626.

Pardoen, T., Hutchinson, J.W., 2000. Extended model for void growth and coalescence. Journal of the Mechanics and Physics of Solids 48 (12), 2467–2512.

Qidwai, M.A., Entchev, P.B., Lagoudas, D.C., DeGiorgi, V.G., 2001. Modeling of the thermomechanical behavior of porous shape memory alloys. International Journal of Solids and Structures 38 (48–49), 8653–8671.

Rebelo, N., Gong, X.-Y., Connally, M., 2003. Finite element analysis of plastic behavior in nitnol. In: SMST-2003: Proceedings of the International Conference on Shape Memory and Superelastic Technologies. SMST Society, Inc., Pacific grove, California, USA, pp. 501–507.

Rice, J.R., Tracey, D.M., 1969. On the ductile enlargement of voids in triaxial stress fields∗. Journal of the Mechanics and Physics of Solids 17 (3), 201–217.

Robertson, S.W., Ritchie, R.O., 2007. In vitro fatigue-crack growth and fracture toughness behavior of thin-walled superelastic nitinol tube for endovascular stents: a basis for defining the effect of crack-like defects. Biomaterials 28 (4), 700–709.

Robertson, S.W., Mehta, A., Pelton, A.R., Ritchie, R.O., 2007. Evolution of crack-tip transformation zones in superelastic nitinol subjected to in situ fatigue: a fracture mechanics and synchrotron x-ray microdiffraction analysis. Acta Materialia 55 (18), 6198–6207.

SIMULIA, 01.07.2010 2010. Answer id 1658: Umat and vumat routines for the elastic-plastic simulation of nitinol.

Søvik, O. 1996. Numerical modeling of ductile fracture – a damage mechanics approach. Ph.D. thesis, NTNU.

Tanaka, K., 1986. A thermomechanical sketch of shape memory effect – one-dimensional tensile behavior. Res Mechanica 18 (3), 251–263.

Tvergaard, V., 1981. Influence of voids on shear band instabilities under plane strain conditions. International Journal of Fracture 17 (4), 389–407.

Tvergaard, V., Needleman, A., 1984. Analysis of the cup-cone fracture in a round tensile bar. Acta Metallurgica 32 (1), 157–169.

Vaidyanathan, R., Dunand, D.C., Ramamurty, U., 2000. Fatigue crack-growth in shape-memory NiTi and niti-tic composites. Materials Science and Engineering A 289 (1–2), 208–216.

Wang, X.M., Lu, Z.Z., Yue, Z.F., 2009. The effect of notches on the fracture behavior in NiTi shape memory alloys. International Journal of Solids and Structures 46 (3-4), 557–571.

Yan, W., Wang, C.H., Zhang, X.P., Mai, Y.W., 2003. Theoretical modelling of the effect of plasticity on reverse transformation in superelastic shape memory alloys. Materials Science and Engineering A 354 (1–2), 146–157.

Zhang, Z.L., Thaulow, C., Ødegård, J., 2000. A complete gurson model approach for ductile fracture. Engineering Fracture Mechanics 67 (2), 155–168.